AIAA JOURNAL
Vol. 35, No. 9, September 1997

Computational Method for Describing Porous Wall Boundary Conditions Based on Experimental Data

Thomas J. Beutner*
Air Force Research Laboratory, Wright–Patterson Air Force Base, Ohio 45433
Zeki Z. Celik†
LSI Logic, Fremont, California 94539
and
Leonard Roberts‡
Stanford University, Stanford, California 94305

A computational and experimental study has been undertaken to investigate methods of modeling solid and porous wall boundary conditions in computational fluid dynamics (CFD) codes. The procedure utilizes experimental pressure measurements at the walls to develop a flow-field solution based on the method of singularities. This solution is then imposed as a pressure boundary condition in a CFD simulation of the internal flowfield. The effectiveness of this method in describing the boundary conditions at the wind-tunnel walls using only sparse experimental measurements has been investigated. Verification of the approach using computational studies has been carried out using an incompressible flow solver. The current work demonstrates this technique for low-speed flows and compares the result with experimental data obtained from a heavily instrumented variable porosity test section. Position and refinement of experimental measurements required to describe porous wall boundary conditions has also been considered for application to other porous wall wind tunnels. The approach developed is simple, is computationally inexpensive, and does not require extensive or intrusive measurements. It may be applied to both solid and porous wall wind-tunnel tests.

Nomenclature

C_p = pressure coefficient
$C_{p_{\text{plenum}}}$ = plenum pressure coefficient
c = airfoil chord
h = wind-tunnel test section height
M = Mach number
n = outward normal coordinate direction
P = porosity parameter
P_L = porosity of lower wall
P_U = porosity of upper wall
p = pressure
p_∞ = freestream pressure
U_∞ = freestream velocity
u, v = two-dimensional Cartesian velocity components
V_0 = empty tunnel normal velocity at walls
x, y = two-dimensional Cartesian coordinates, origin at airfoil leading edge where α is zero
x_0, y_0 = position of two-dimensional singularities
α = angle of attack
β = $\sqrt{(1 - M^2)}$
γ = two-dimensional vortex strength
μ = two-dimensional x-doublet strength
σ = two-dimensional source strength
ϕ = perturbation velocity potential
ω = two-dimensional y-doublet strength

Introduction

VENTILATED wall wind tunnels have been in use for several decades and have been useful in reducing wall interference effects at subsonic and transonic speeds and allowing for testing through Mach 1. A series of improvements have been made to the earliest ventilated wind tunnels leading to modern porous wall test sections.

It has long been recognized that the corrections to wind-tunnel data for open and closed test sections were of opposite signs.[1] Theodorsen[2] suggested that a wind tunnel might be constructed that would reduce wind-tunnel wall interference by using a partially open wall. Wright and Ward[3] tested one of the first successful ventilated wall wind tunnels, which used several streamwise slots in the tunnel walls. As predicted, they found that blockage interference was reduced. Wright and Ward also found that ventilated walls alleviated the choking problems at transonic speeds and permitted testing through Mach 1. It was soon realized, however, that streamwise slots allowed for reflection of shock and expansion waves from the tunnel walls.[4] Porous wall tunnels, constructed with a pattern of small discrete holes through the walls, alleviated this problem by significantly reducing the shock and expansion wave reflections from the walls.[5] The differential resistance wall was a further refinement to the porous wall concept, using holes with the hole axis inclined to the normal, to improve the inflow and outflow characteristics of the porous wall.[1]

Motivation for Modeling the Porous Wall Boundary Condition

As high-speed computers have increased the flexibility and capability of computational modeling of flowfields, a new emphasis has been placed on obtaining wind-tunnel data that may be used to calibrate and validate computational fluid dynamics (CFD) codes.[6] Increasingly, there has been a trend toward modeling entire wind-tunnel flowfields, including support struts and wind-tunnel walls.[7,8] This has led to an increased use of solid walls in wind-tunnel testing. The simplicity of modeling a solid wall boundary condition has made their use attractive despite the disadvantages of substantial wall interference.[9] Increased emphasis on high Reynolds number testing in existing facilities[10,11] and increasing use of CFD codes for high Reynolds number applications, however, are creating a renewed incentive for porous wall wind-tunnel testing. When solid wall tunnels are used for these tests, wall interference can become a limiting condition on the size of models. Additionally, ventilated wall tunnels are useful for low-speed tests where significant wall interference is present.[12]

Received July 26, 1996; revision received April 28, 1997; accepted for publication April 30, 1997.

*Aerospace Engineer, Experimental Operations and Diagnostics Branch. Senior Member AIAA.
†Engineer, Characterization and Simulation Department. Member AIAA.
‡Professor Emeritus, Department of Aeronautics and Astronautics. Fellow AIAA.

While allowing larger models to be tested, porous walls may also eliminate shock wave reflections from the walls of the test section. This is significant in many cases where the reflected shock may impinge on the model. Thus, the use of porous wall data for CFD comparisons may reduce the grid refinement required near the wind-tunnel walls while providing a more realistic assessment of the code capability for free air calculations.

Some attempts have been made to model discrete slots in CFD codes either by modeling the slots in an approximate manner or by solving coupled equations to describe the boundary condition.[13,14] Porous walls, which may have several thousand intricate holes, are more difficult to model in CFD calculations. Modeling the individual holes and the viscous effects associated with each hole in a CFD grid is not possible given the current limitations on computer speed and memory. Thus, the effect of the porous walls must be dealt with either by correcting the test data to free air conditions or by modeling the porous wall by appropriate means in the CFD code.

Previous Models for the Porous Wall Boundary

Numerous approaches for correcting porous wall data to free air conditions have been proposed. These methods use a variety of approaches, based on model pressure and force measurements,[15] wall boundary pressure or velocity measurements, or pressure rail measurements.[1,16] These methods generally produce a global correction to the velocity and angle of attack, with additional corrections for drag and moment coefficients and Mach number sometimes included. These methods are generally based on classical reflection techniques incorporating a linearized boundary condition to account for the porous wall. This approach results in a useful comparison of bulk flow measurements, such as lift and drag coefficients, but these methods are of limited use in performing CFD comparisons because they have the effect of altering the entire flowfield. Thus, errors resulting from the corrections may be attributed to the CFD calculation, and a comparison of the entire flowfield is not possible. Other approaches have sought to develop a boundary condition that may be used at the ventilated wall boundary in the CFD code. These methods have depended on a simple, universal boundary condition, on detailed measurements of the boundary conditions during wind-tunnel tests, which were then imposed as a boundary condition in the CFD code, or on an integrated boundary-layer analysis based on wall calibrations and experimental measurements.[17–22]

A universal boundary condition for porous walls has proven difficult both to determine experimentally and to implement computationally. The linear boundary condition proposed by Baldwin et al.[5] (also see Ref. 1) has proven useful in performing corrections to porous wall data and gives some insight into the behavior of the porous wall, but it does not appear adequate to describe porous walls in a CFD code. The porosity parameter in this boundary condition may be different for otherwise identical top and bottom walls, and it may depend on Mach number, stagnation pressure, model size, and orientation.[23] This may result in extensive measurements being required for each test condition in order to determine an appropriate value for the porosity parameter. Additionally, there is evidence that the linear relationship between pressure coefficient and flow inclination implied by such a boundary condition does not exist over the entire wall.[19] This casts doubt on the appropriateness of applying such a linear boundary condition in CFD simulations. Furthermore, such a boundary condition may be destabilizing in CFD codes and can actually prevent convergence. Still, the linear boundary condition gives some valuable insight into the nature of the flow near a porous wall.

Some current efforts in ventilated wall interference research have been directed toward making detailed measurements of the flow near the walls and using these measurements to prescribe a boundary condition in CFD codes. King and Johnson[17,18] used detailed pressure measurements on a surface midway between the model and wall to prescribe a pressure boundary condition in a two-dimensional CFD simulation of a slotted wall test. Jacocks[19] used a detailed calibration of a porous wall tunnel, along with detailed measurements during wind-tunnel tests to develop an equivalent inviscid normal velocity profile based on an integrated boundary-layer analysis. An extension of this method has also been developed by Crites and Rueger[20] and applied to limited three-dimensional problems.[21,22] These approaches typically require measurements of the wall boundary conditions and significant effort for calibration of the ventilated wall flow characteristics at each open area ratio, plenum pressure, Mach number, and Reynolds number to develop an integrated boundary-layer solution for the flow near the wall, which is then imposed as a boundary condition in the CFD solution.

Current Approach

The approach presented here represents an attempt to describe the effects of a porous wall boundary in a CFD code based on sparse, easily obtained, pressure measurements on the wind-tunnel wall. The approach is noniterative, is robust enough to handle cases in which only limited data from the walls are available, and does not require calibrations of the wall crossflow characteristics. The application of the pressure boundary condition in the CFD simulation can be achieved without compromising stability or convergence rates. The usefulness of this approach was demonstrated by carrying out wind-tunnel experiments in a heavily instrumented variable porosity research tunnel and performing CFD simulations of the experiments.

The approach to describing the porous wall boundary condition utilized classical porous wall theory as a means of interpolating boundary conditions measured during wind-tunnel tests. A solution for the flow near the walls, based on the method of singularities, was developed using measurements made on the walls during wind-tunnel tests. The singularity solutions used in this method satisfied the classical porous wall boundary condition and served as basis functions for the flow solution. Singularity strengths were determined by means of a least squares fit to streamwise velocities at the wind-tunnel walls, inferred from static pressure measurements made on the walls. The method of singularities solution was then used to specify the pressure at CFD boundary point locations. This approach requires very few measurements to determine the flowfield solution, although it makes use of all available data and accuracy improves with the number of measurements used.

The current work consists of experimental studies conducted in the Stanford low-speed wind tunnel and computational studies performed using an incompressible flow solver. Although the Mach number range for this facility was very low, some consideration has been given to the implementation of this method for higher speed flows, and a series of computational experiments has indicated that the boundary condition may be applied in transonic CFD simulations.

Experimental Facilities

This research used a low-speed, heavily instrumented, variable porosity test section, which was built and tested at the Stanford University low-speed wind tunnel (Fig. 1). Nominal freestream velocity for these tests was 24 m/s and the Reynolds number based on airfoil chord was 3.2×10^5.

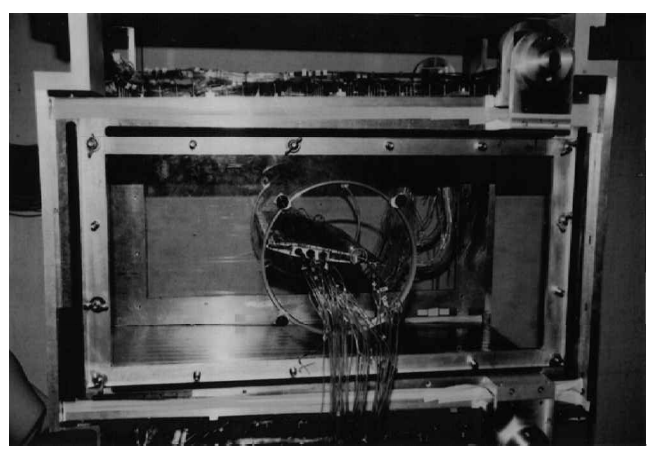

Fig. 1 Variable porosity test section with airfoil model installed.

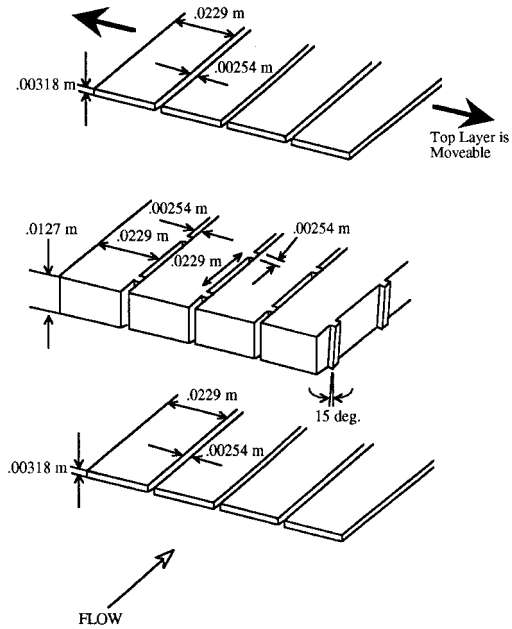

Fig. 2 Exploded view of variable porosity wall.

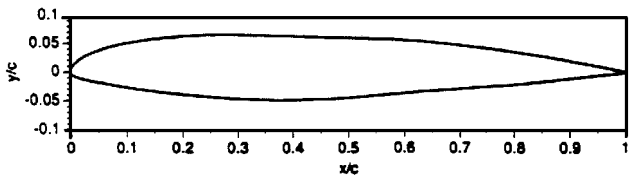

Fig. 3 Boeing advanced transport airfoil cross section.

The test section was 0.457 × 0.457 m and the porous portion of the test section was 0.76 m long. An atmospheric breather section was located at the end of the test section. The porous walls of the test section were layered in a design that used porous inserts between two longitudinally slotted layers of the wall. The outer slotted layer of each wall could be slid laterally to vary the open area ratio of the wall from a solid wall condition to an open area ratio of 9%. Figure 2 shows an exploded view of this wall design. An atmospheric plenum was used for all porous wall tests. The test section top and bottom walls were adjustable and were inclined normal to the freestream to compensate for boundary-layer growth through the test section.

For two-dimensional testing, variable porosity top and bottom walls were used, and solid side walls were used with the airfoil model mounted to the side walls. The airfoil used in the tests was a Boeing advanced transport airfoil and may be seen in Fig. 3. The model had a flap and spoiler, which were in the retracted position for these tests. The airfoil chord was 0.203 m. Measurements of the model coordinates were made with a Leitz precision measuring machine with an accuracy of 2.54×10^{-6} m, or approximately 0.00125% of the airfoil chord. Grit was applied to the airfoil between 2.5 and 5.0% of the chord. Nominal grit diameter was 3.18×10^{-4} m. Oil flow studies were undertaken to ensure the two dimensionality of the flowfield on the airfoil model and to ensure that the grit applied to the model successfully triggered transition on the airfoil.

The test section was instrumented with 77 static pressure tappings on the centerlines of the upper and lower walls, and a total of 482 static pressure tappings distributed over the upper and lower walls. Pressure tappings were also located on the model. The test section design also allowed five-hole probe access near the upper and lower walls and on the inflow and outflow planes. The five-hole probe was used to determine flow inclinations and velocity perturbations on these planes.

Static pressure data were acquired by three Scanivalves, which were calibrated on each run against a secondary standard that was traceable to the National Bureau of Standards. Maximum uncertainties in pressure coefficient measurements were calculated by the linear equation method[24] to be ± 0.005.

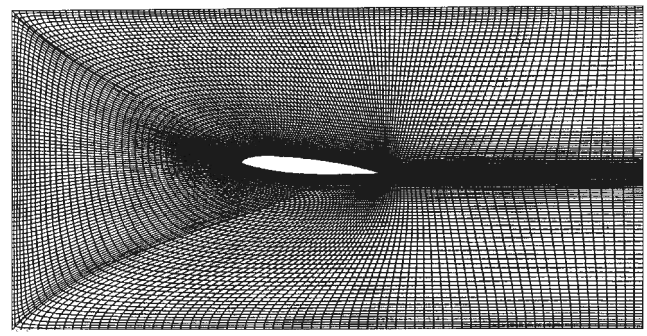

Fig. 4 Example of 250 × 70 grid used for 5-deg-angle-of-attack case.

Computational Methods

Navier–Stokes Solver

The INS2D code, a two-dimensional, incompressible, Reynolds-averaged Navier–Stokes solver[25] developed at NASA Ames Research Center, was used in this study. This CFD code solved the incompressible Navier–Stokes equations using the method of artificial compressibility. The method of artificial compressibility adds a pseudotime derivative of pressure to the continuity equation. This results in a hyperbolic system of equations, which may be marched in pseudotime to a steady-state solution.[26] A Baldwin–Barth turbulence model[27] was used, and the transition point was fixed at the airfoil leading edge. This code was fully implicit, used a third-order accurate locally upwind differencing of the convective fluxes, and used a second-order accurate central differencing of the viscous fluxes. The code was modified to allow for an experimental static pressure profile to be imposed as a boundary condition for internal flow calculations. On the boundaries where the pressure was specified, velocity components were obtained by the method of characteristics, as implemented in the solver.[25] All computations were performed on the Cray Y-MP at NASA Ames Research Center.

Grids used in this flow solver were C-grids, which conformed to the boundaries of the test section (Fig. 4) and were developed using GRIDGEN software.[28] Nominal grid dimensions were 250 × 70, although a test case was run using a 350 × 105 grid to examine the effect of grid refinement in the solutions. Surface definitions were based on spline fits to approximately 2000 measurements of the model geometry. The very high resolution of measured model geometry allowed for excellent geometry definition in the grids, as well as resolution of model surface discontinuities associated with the flap and spoiler attachment.

Method of Singularities

As a means of describing the wind-tunnel wall boundary conditions in a wind-tunnel experiment, a potential flow solver based on the method of singularities was developed.

The boundary condition of the following equation has been proposed as a theoretical description of a porous wall boundary[1]:

$$\frac{\partial}{\partial x}\phi + \frac{1}{P}\frac{\partial}{\partial n}\phi = \frac{1}{P}\frac{V_0}{U_\infty} - \frac{1}{2}C_{p_{\text{plenum}}} \tag{1}$$

The boundary condition of Eq. (1) assumes an analogy between flow through the porous wall and flow through a pipe. Velocities normal to the wall are assumed to be linearly related to the pressure difference existing across the wall. The pressure differences across the wall are, in turn, related to the perturbations in the tangential velocity at the wall. The right-hand-side terms in Eq. (1) account for the flow through the wall, which is observed during empty tunnel runs. In theory, $V_0 = 0$ when holes are normal to the tunnel wall. However, porous wall tunnels generally use holes inclined to the normal direction in order to improve inflow and outflow characteristics. Inclined holes may have the effect of inducing a velocity V_0 through the walls even during empty tunnel tests. In practice, however, V_0 may be negligibly small and is often neglected. The second term on the right-hand side of Eq. (1) accounts for the pressure difference created by the porous wall plenum. If the plenum pressure is chosen to be the freestream static pressure, the second term is

zero. If the right-hand-side terms in Eq. (1) are both neglected, the homogeneous boundary condition of Eq. (2) results:

$$\frac{\partial}{\partial x}\phi + \frac{1}{P}\frac{\partial}{\partial n}\phi = 0 \tag{2}$$

As mentioned earlier, the porosity parameter P in Eq. (2) must be determined from experimental measurements. It is generally assumed that the porosity parameter is constant over the length of the porous wall. Some of the limitations of this boundary condition have already been mentioned, and these limitations make direct application of Eq. (2) as a boundary condition in CFD codes questionable.

Despite the difficulties in applying Eq. (2) directly as a boundary condition in porous wall CFD simulations, the insight it provides into the nature of the flow near a porous wall makes it useful for interpolating experimental data.

Analytic solutions for the perturbation velocity potentials due to a source, a vortex, and doublets, i.e., derivatives of the source and vortex, in the presence of porous walls described by Eq. (2) have been developed[1] and are shown in Eqs. (3–12). Higher-order singularities may be developed by taking additional derivatives of the expressions in Eqs. (5) and (6).

Source:

$$\phi_\sigma = (\sigma/\beta)[B(Z) + E(Z) + \chi(P_U)\chi(P_L)] \tag{3}$$

Vortex:

$$\phi_\gamma = i\gamma[B(Z) - E(Z)] \tag{4}$$

X-doublet:

$$\phi_\mu = \frac{\mu}{\beta^2 h}\frac{\mathrm{d}}{\mathrm{d}Z}[B(Z) + E(Z)] \tag{5}$$

Y-doublet:

$$\phi_\omega = \frac{i\omega}{\beta h}\frac{\mathrm{d}}{\mathrm{d}Z}[B(Z) - E(Z)] \tag{6}$$

where

$$Z = (x/\beta h) + (iy/h) \tag{7}$$

$$Z_0 = (x_0/\beta h) + (iy_0/h) \tag{8}$$

$$B(Z) = \frac{1}{2}\frac{\exp\{\pi[(\tau_U + \tau_L)/2](Z - Z_0)\}}{\exp[\pi(Z - Z_0)] - 1} \tag{9}$$

$$E(Z) = -\frac{1}{2}\frac{\exp\{\pi[(\tau_U + \tau_L)/2](Z - \bar{Z}_0)\}}{\exp[\pi(Z - \bar{Z}_0)] + 1}\cdot\exp\left[i\pi\frac{\tau_U - \tau_L}{2}\right] \tag{10}$$

$$\chi(P_U)\chi(P_L) = \begin{cases} 1, & \text{if} \quad P_U = P_L = 0 \\ 0, & \text{otherwise} \end{cases} \tag{11}$$

$$\tau_{U,L} = (2/\pi)\,A\tan(P_{U,L}/\beta) \tag{12}$$

The approach used in this research was to use experimental pressure data to develop a potential flow solution, and then to use this potential flow solution to develop a pressure boundary condition for the CFD calculation. This allowed a means of interpolating sparse wind-tunnel boundary condition measurements onto the computational grid. The singularities used were a point source and a point vortex, described earlier, and derivatives of the point source and point vortex, i.e., doublets, quadruplets, etc. Up to four derivatives were retained in the potential flow solution. Singularity strengths were determined by making a least squares fit of the velocity profiles due to the singularities and the streamwise velocity profiles inferred from static pressure measurements on the wind-tunnel walls. The potential flow solution was then used to prescribe pressure boundary conditions in the CFD code. Thus, sparse data could be interpolated and extrapolated using the method of singularities. Although the singularities used in this method satisfied the boundary condition of Eq. (2), only the pressure profile resulting from the potential flow solution was specified in the CFD code. Thus, the difficulties of using Eq. (2) as a direct boundary condition in CFD calculations could be avoided.

Previous work by the authors has shown how this method may be applied in three dimensions.[29] Although analytical solutions for three-dimensional singularities satisfying the boundary condition of Eq. (2) are not available, these solutions may be obtained by simple panel methods. Previous work by the authors has also shown, by a series of computational studies, that this method may be applied in transonic flow solvers.[30]

Boundary Conditions

In the CFD comparisons performed in this research, the top and bottom wall boundary conditions were static pressure boundary conditions. The static pressure profiles on these walls were determined by the method of singularities already described. The outflow plane also used a static pressure boundary condition based on the breather section pressure. For both the walls and the outflow plane, the remaining flow variables were solved for by the method of characteristics, as implemented in the INS2D code.

On the inflow plane, the velocity profile was specified. This velocity profile was based on a cubic polynomial fit to the five-hole probe velocity measurements on the inflow plane. Pressure on the inflow plane was determined by the method of characteristics. A no-slip boundary condition was used on the airfoil, and averaging was used on the wake cut.

Evaluation of Method

Previous computational studies by the authors with a transonic CFD code have demonstrated this method and the consistency of the pressure boundary condition as a means of describing a wall boundary condition in a flowfield containing shocks, provided the shocks do not impinge on the wall.[30] In that work as in the current work, pressure was specified as a boundary condition with the remaining flow variables solved for by the method of characteristics. Previous work[29,31] also showed that the method described here is relatively insensitive to changes in the porosity parameter P. The value of P in this work was determined by minimizing the root-mean-square error in matching wall velocity profiles.

The evaluation of this technique for describing a wind-tunnel boundary condition was broken into two parts. First, the method of singularities was evaluated in a series of computational studies. Second, the method was used to perform CFD comparisons using experimental data obtained from the variable porosity test section.

The computational studies were centered on evaluating the number of data points and the number of singularities required to adequately describe the boundary conditions. This study was performed by using a CFD simulation in which slip wall boundary conditions were used at the tunnel wall boundaries. This CFD simulation was treated as a pseudowind-tunnel experiment, and data samples, which were representative of measurements obtainable from wind-tunnel tests, were taken from the boundaries of this CFD simulation. Various numbers of data points were used to develop potential flow solutions, and these potential flow solutions were then compared to the original, complete velocity profiles from the CFD simulation. Using a computational study for this evaluation had the advantage of allowing more detailed comparisons of the boundary conditions on the walls than would be possible using experimental data only.

The second part of the evaluation of this method involved using experimental wall pressure profiles from both solid and porous wall tests to develop flowfield solutions with the method of singularities. These flowfield solutions were then imposed as a pressure boundary condition in the CFD code. CFD simulations were carried out for solid wall and porous wall (9% open area ratio) tests[29,31] at angles of attack from 5 to 11 deg. These simulations used boundary conditions developed by the method of singularities using a source, a vortex and four derivatives of each to develop a pressure profile based on a total of 77 pressure measurements on the wind-tunnel walls.

As a further test of this method, the method of singularities was used to develop pressure profiles based on very sparse data from the wind-tunnel test. For these cases, a total of eight data points from the

wind-tunnel tests were used to develop the method of singularities solution. This solution was then imposed as a boundary condition in the CFD code, and the resulting pressure profiles on the airfoil were compared with the results obtained using more complete data from the wind-tunnel tests. This allowed for an evaluation of the robustness of this approach when only limited data are available to determine the wind-tunnel boundary conditions.

Comparisons to CFD calculations using alternate methods of specifying the wall boundary condition were also made. For these cases, the solid wall was modeled in three different ways: 1) with the pressure boundary condition based on the method of singularities fit to the experimental data, 2) as a slip wall boundary condition imposed at the nominal boundary-layer edge, as measured experimentally, and 3) as a no-slip boundary condition, on a refined grid, which conformed to the physical wall location.

Results

Figure 5 shows the pressure profiles on the walls as predicted by the CFD simulation using slip wall boundary conditions for an angle of attack of 5 deg. This simulation was used to determine the effects of refining the number of data points used to develop the potential flow solution.

Figure 6 shows the rms error resulting when various numbers of data points were used to develop the potential flow solutions. These data points were distributed as uniformly as grid spacing would allow over the top and bottom walls. The rms errors were based on a comparison of the pressure predicted by the CFD simulation and the pressure predicted by the potential flow solver at each grid point on the upper and lower walls. As may be seen in Fig. 6, a relatively small number of measurement locations was sufficient to develop a suitable potential flow solution. In addition, a small number of singularities was adequate to describe the far-field flow with good accuracy.

Additional singularities required additional data points to produce acceptable fits to the velocity profiles. It was found that the number of data points required to produce a good fit to the velocity profiles was approximately twice the number of singularities retained in the potential flow solution.

The next step in evaluating this method was to use it to perform comparisons to a series of wind-tunnel tests. The tests were conducted in the variable porosity tunnel described earlier. Results for experiments and calculations for 8-deg angle of attack are shown in Fig. 7. Figure 7 shows data from both the solid wall tests and the porous wall tests with a 9% open area ratio. Also shown in Fig. 7 are the potential flow solutions based on these data. The potential flow solutions were developed using the 77 measurements on the centerline of the wind tunnel walls and a total of 10 singularities, i.e., a source, a vortex, and four derivatives of each. The potential flow solutions showed excellent agreement with the experimental data. Typical rms errors in matching wall pressure coefficient profiles were approximately 1% of peak pressure coefficient values.

The potential flow solutions shown in Fig. 7 were imposed as boundary conditions in the Navier–Stokes solver, and the resulting pressure profiles obtained on the airfoil are shown in Fig. 8. As in Fig. 7, both solid and porous wall cases are shown in Fig. 8. Also shown in Fig. 8 are the pressure profiles on the airfoil obtained in the wind-tunnel tests. Experimental and computational results compared very well. The largest discrepancies were approximately 6% of the peak values. These discrepancies occurred at the location of the grit transition strip on the model. At locations away from the grit strip, however, agreement was much better with discrepancies of approximately 1% of peak values. A comparison of airfoil pressure profiles from the solid wall and porous wall tests showed that this method predicted the effect of a porous wall very well. As the porosity of the wall was varied, the trend in pressure profiles on the airfoil was duplicated in the CFD simulations by imposing the potential flow solution as a pressure boundary condition in the Navier–Stokes solver.

Also of interest in Fig. 8 are the slight deviations seen in the pressure profiles on the airfoil between $x/c = 0.75$ and 0.80. These deviations may be seen on both the upper and lower surfaces and are present in both the experimental and CFD data. They are the result of small ridges on the airfoil model between the main airfoil and the retracted flap.

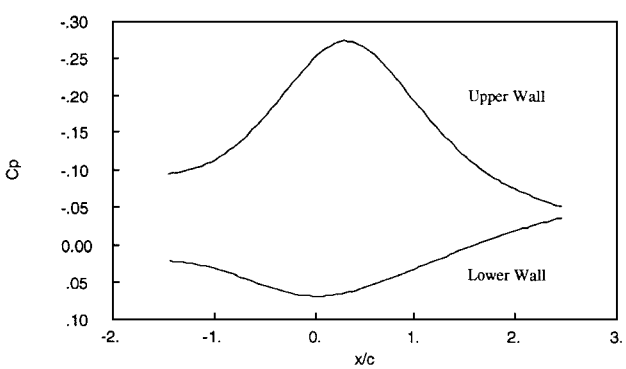

Fig. 5 Pressure profiles on the upper and lower walls predicted by the Navier–Stokes solver using a slip wall boundary condition.

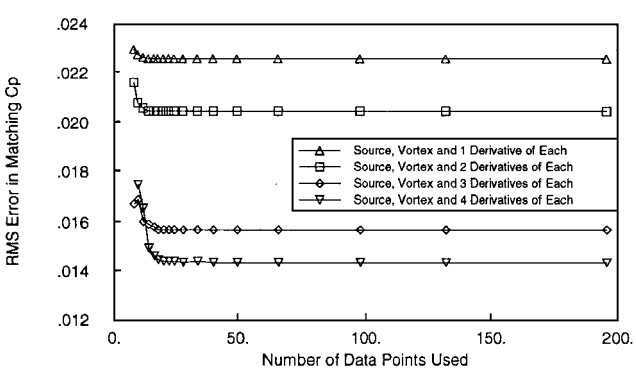

Fig. 6 RMS errors as a function of the number of data points used to develop the method of singularities solution and the number of singularities retained.

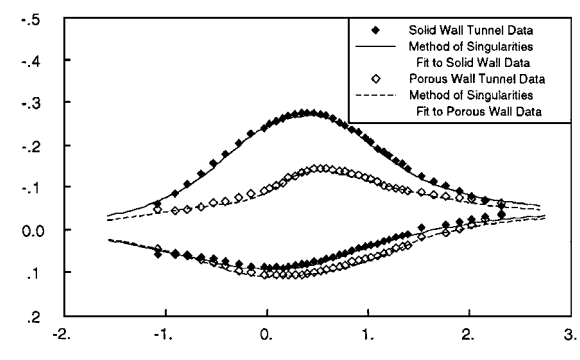

Fig. 7 Method of singularities matches to the pressure profiles on the upper and lower walls for $\alpha = 8$ deg; experimental data, and singularity solutions shown for both solid wall case and the 9% open area ratio porous wall.

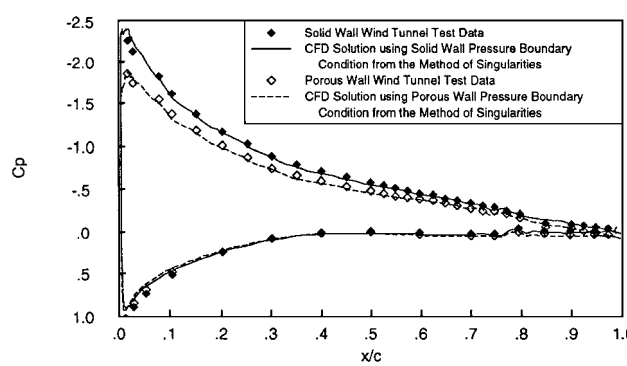

Fig. 8 Comparison of experimental and CFD pressure profiles on the airfoil for $\alpha = 8$ deg case; both solid and porous wall results are shown.

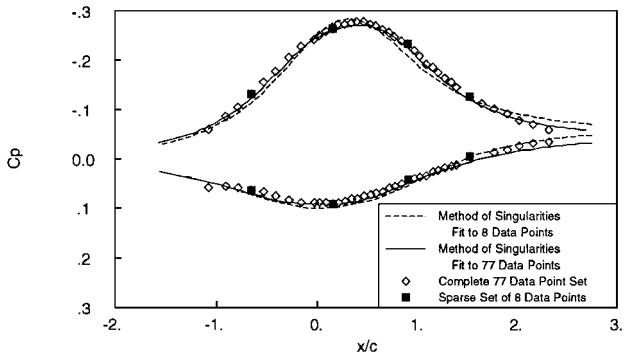

Fig. 9 Comparison of the method of singularities fit to the complete set of data and to a sparse set of data (eight data points) for the solid wall, $\alpha = 8$ deg case.

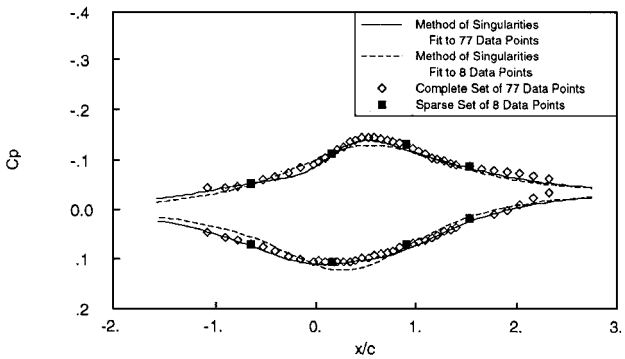

Fig. 10 Comparison of the method of singularities fit to the complete set of data and to a sparse set of data (eight data points) for the porous wall, $\alpha = 8$ deg case.

Figures 9 and 10 show typical results obtained by using sparse data to develop the potential flow solutions. Figure 9 shows the potential flow solution developed using 8 data points from the solid wall test at 8-deg angle of attack. Figure 10 shows similar results for the porous wall data case at 8-deg angle of attack. In these cases, only first derivatives were retained in the singularity solution, resulting in a total of four singularities being used to develop the pressure profiles shown. In both Figs. 9 and 10, the complete wind-tunnel data sets are shown for reference, as well as the potential flow solutions based on the complete wind-tunnel data set. The potential flow solutions based on only 8 data points show close agreement with the potential flow solutions based on the complete set of 77 data points. Typical rms errors in matching the complete experimental pressure coefficient profiles using the method of singularities solution based on 8 data points were approximately 10% of peak values. Although these errors were higher than the cases in which 77 data points were used to develop the solution, the trend of the pressure profiles is still captured using very sparse data. This agreement indicates that this method was robust enough to allow for a good description of the boundary conditions on the walls even when only very sparse data was available from the wind-tunnel walls. As indicated earlier, agreement improves with increasing number of measurements available on the wind-tunnel walls.

The pressure profiles shown in Figs. 9 and 10 were imposed as boundary conditions in the CFD code, and the resulting pressure profiles on the airfoil are shown in Figs. 11 and 12. For reference, the airfoil pressure profiles that resulted by imposing the boundary conditions of Fig. 7 in the CFD code are also shown in Figs. 11 and 12. This allows a comparison of the effect on the airfoil of using sparse data to develop the wall boundary conditions. As can be seen, the method of singularities provided a means of describing boundary conditions that was sufficiently robust so that little effect was seen on the airfoil from significantly reducing the number of measurements used to develop the wall boundary conditions. Typical rms errors between the pressure coefficient profiles shown in Figs. 11 and 12 was 1.5% or less of the peak values for the range of angles of attack tested.

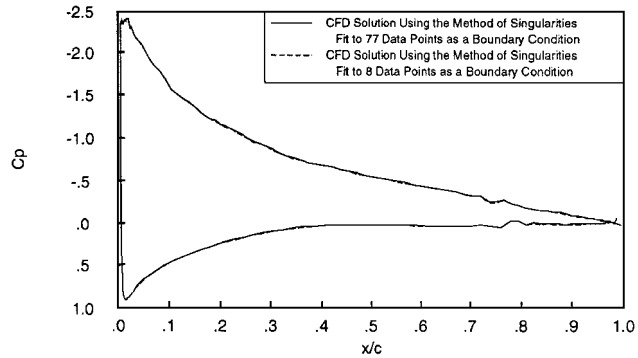

Fig. 11 Comparison of CFD pressure profiles on the airfoil obtained using the boundary conditions developed from sparse and fine data (shown in Fig. 9).

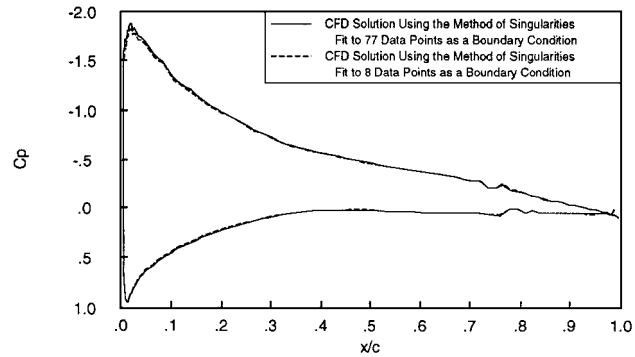

Fig. 12 Comparison of CFD pressure profiles on the airfoil obtained using the boundary conditions developed from sparse and fine data (shown in Fig. 10).

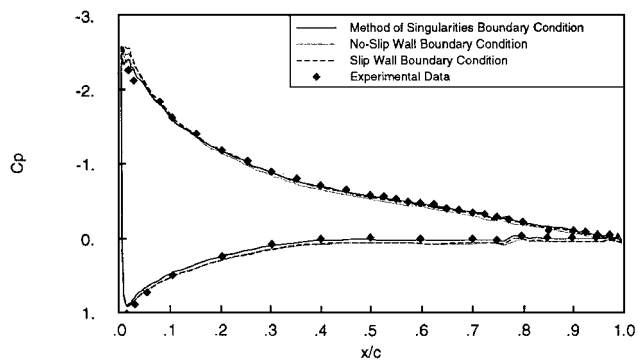

Fig. 13 Comparison of pressure profiles on the airfoil from CFD simulations using a specified pressure boundary condition, a no-slip wall boundary condition, and a slip wall boundary condition.

Finally, a comparison was made to other methods of describing a solid wall boundary condition. Figure 13 shows a comparison of CFD results obtained using the method of singularities boundary condition, a slip wall boundary condition imposed at the nominal wall location (the edge of the boundary layer), and a no-slip wall boundary condition imposed on a refined grid, which resolved the boundary layer on the wall. Experimental data are also shown. Good agreement between the three methods indicates that the method of singularities is suitable for modeling the wall boundary condition.

In all of the preceding cases, both the singularity strengths and the porosity parameter were chosen to minimize the least squares error between the singularity solution and the experimental data. In all cases, the optimum porosity parameter was found to be $P = 0$. Figure 14 shows a typical variation of the rms error in matching the C_p on the wall boundaries as a function of the value of the porosity parameter. In this figure the rms errors have been normalized by the peak C_p value on the walls. It is notable that the curves are discontinuous at $P = 0$. This discontinuity has been well documented[1] and results from the source term being developed

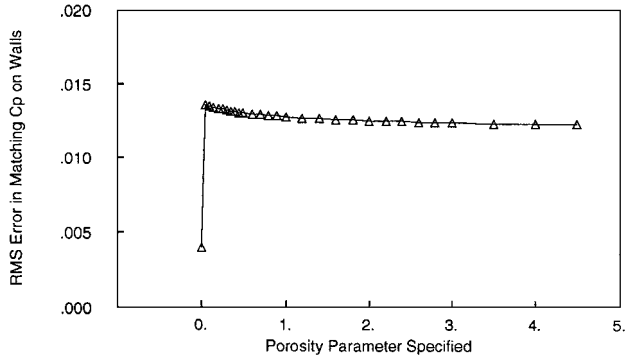

Fig. 14 RMS errors in matching the wall pressure profiles, as a function of the porosity parameter *P* specified in the method of singularities; experimental data for this comparison were from the porous wall, $\alpha = 8$ deg case.

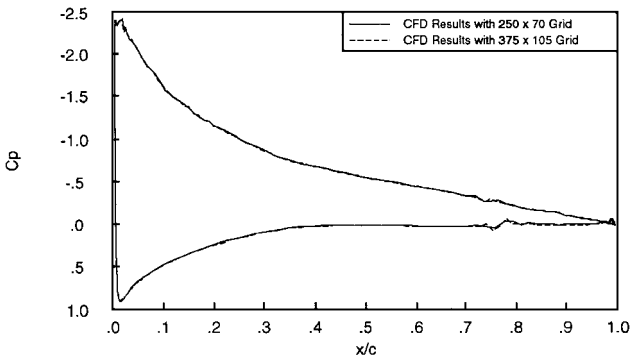

Fig. 15 Airfoil pressure distributions obtained with the nominal and refined grids.

based on infinite strip theory. For the solid wall case, a bias is introduced so that the mass added by the source exits downstream, at infinity [see Eq. (11)]. For the porous wall case, no matter how small the porosity, the mass addition from the source will leak out through the walls. This discontinuous behavior is apparent in Fig. 14. However, it is notable that, at least in this low-speed case, an arbitrary choice of the porosity parameter still results in an acceptable fit to the experimental data.

Grid resolution studies conducted early in the investigation indicated that the chosen grids were sufficiently refined so that additional grid refinement had little effect on the solution. For comparison purposes, an additional result was computed on a 350×105 grid, using approximately twice the number of grid points as the standard grid. Figure 15 shows the comparison of the results obtained on the airfoil for the two cases of the 350×105 grid and the 250×70 grid. Some effects of the additional refinement are evidenced near the flap and spoiler ridges on the aft portion of the airfoil, but overall results indicated that the 250×70 grid was sufficiently refined so that remaining errors associated with grid refinement were minimal.

Concluding Remarks

A method for describing porous wall boundary conditions based on sparse, nonintrusive measurements of static pressure at the wall boundary has been developed. This method utilized a potential flow solution based on least squares matching of singularity strengths to measured experimental data. The consistency of imposing a pressure boundary condition based on this method with other means of describing a wall boundary condition has been demonstrated in computational studies. This method has been shown to provide a good description of the entire wall boundary condition even when only sparse data is available. The ability of this method to predict the effects of changing porosity in a wind-tunnel test has been demonstrated by simulation of experiments performed in a variable porosity test section.

In these low-speed tests, the method of singularities has been found to be rather insensitive to the value of the porosity parameter specified. This allowed for the porosity parameter to be found by means of least squares matching. Although changes in the porosity parameter did have a strong effect on the singularity strengths, the effect on the overall match to the pressure profile was minimal. Because the porosity parameter was not specified as a boundary condition in the CFD code, and no corrections were made to the wind-tunnel data, this method eliminated many of the concerns associated with the classical linear porous wall boundary condition. This method also allowed for a simulation of the entire flowfield and direct comparison of the flowfield to wind-tunnel data without the need for corrections to the experimental data.

Acknowledgments

This work was performed at Stanford University and was supported by a research Grant NCC 2-55 from NASA Ames Research Center. Additional support has been provided for the Ph.D. thesis work associated with this research by the Air Force Palace Knight program. The authors gratefully acknowledge the help of Stuart Rogers and Mark Potsdam in computational aspects of this work.

References

[1]Mokry, M., Chan, Y. Y., and Jones, D. J., "Two-Dimensional Wind Tunnel Wall Interference," AGARD Rept. AG-281, Nov. 1983, pp. 1–79.

[2]Theodorsen, T., "The Theory of Wind-Tunnel Wall Interference," NACA TR-410, Dec. 1932, pp. 219–227.

[3]Wright, R. H., and Ward, V. G., "NACA Transonic Wind-Tunnel Test Sections," NACA TR 1231, Jan. 1956, pp. 623–636, 659, 660.

[4]Ritchie, V. S., and Pearson, A. O., "Calibration of the Slotted Test Section of the Langley 8-Foot Transonic Tunnel and Preliminary Experimental Investigation of Boundary Reflected Disturbances," NACA RM-L51K14, July 1952, pp. 12–22.

[5]Baldwin, B. S., Turner, J. B., and Knechtel, E. D., "Wall Interference in Wind Tunnels with Slotted and Porous Boundaries at Subsonic Speeds," NACA TN-3176, May 1954, pp. 1–29.

[6]Marvin, J. G., "Accuracy Requirements and Benchmark Experiments for CFD Validation," AGARD CP-437, Paper 2, May 1988.

[7]Lan, C. E., and Thomas, J. P., "Application of Computational Aerodynamics to Assessment/Correction in Wind Tunnel Testing," Univ. of Kansas Center for Research, Inc., Rept. KU-FRL-887-1, Lawrence, KS, Sept. 1990, pp. 8–30.

[8]Levy, L. L., "Experimental and Computational Steady and Unsteady Transonic Flows About a Thick Airfoil," *AIAA Journal*, Vol. 16, No. 6, 1978, pp. 564–572.

[9]Potsdam, M., and Roberts, L., "A Numerical Study of the Effects of Wind Tunnel Wall Proximity on an Airfoil Model," Dept. of Aeronautics and Astronautics, JIAA TR-99, Stanford Univ., Stanford, CA, Sept. 1990, pp. 36–56.

[10]Lynch, F. T., "Experimental Necessities for Subsonic Transport Configuration Development," AIAA Paper 92-0158, Jan. 1992.

[11]Olson, L. E., "Future Experimental Needs in Low Speed Aerodynamics," AIAA Paper 92-0157, Jan. 1992.

[12]Shujie, W., Yuan, R., and Ruiqin, C., "Investigation of Wall Interference at High Angle of Attack in a Low Speed Wind Tunnel with Slotted Wall," AIAA Paper 87-2611, Aug. 1987.

[13]Agrell, N., and Pettersson, B., "Numerical Computations and Measurements of Transonic Flow in a Slotted-Wall Wind Tunnel," AIAA Paper 87-2610, Aug. 1987.

[14]Al-Saadi, J. A., and DeJarnette, F. R., "Wall Interference Calculation in a Transonic Test Section Including Simulation of Discrete Slots," AIAA Paper 92-0032, Jan. 1992.

[15]Rizk, M. H., and Lovell, D. R., "Euler Procedure for Correcting Two-Dimensional Transonic Wind-Tunnel Wall Interference," *AIAA Journal*, Vol. 26, No. 12, 1988, pp. 1457–1466.

[16]Gopinath, R., "Wall Interference Evaluation from Pressure Measurements on Control Surfaces," *Journal of Aircraft*, Vol. 19, No. 12, 1982, pp. 1097,1098.

[17]King, L. S., and Johnson, D. A., "Calculations of Transonic Flow About an Airfoil in a Wind Tunnel," AIAA Paper 80-1366, July 1980.

[18]King, L. S., and Johnson, D. A., "Transonic Airfoil Calculations Including Wind Tunnel Wall-Interference Effects," *AIAA Journal*, Vol. 24, No. 8, 1986, pp. 1378–1380.

[19]Jacocks, J. L., "An Investigation of the Aerodynamic Characteristics of Ventilated Test Section Walls for Transonic Wind Tunnels," Ph.D. Dissertation, Dept. of Aeronautical Engineering, Univ. of Tennessee, Knoxville, TN, Dec. 1976, pp. 36–51, 56–69.

[20]Crites, R., and Rueger, M., "Modeling the Ventilated Wind Tunnel Wall," AIAA Paper 92-0035, Jan. 1992.

[21]Rueger, M., and Crites, R., "Wind Tunnel Boundary Interference Prediction and Correction," AIAA Paper 92-0036, Jan. 1992.

[22]Rueger, M., Crites, R., Weirich, R., Creasman, F., Agarwal, R., and Deese, J., "Transonic Wind Tunnel Boundary Interference Correction," *Wall Interference, Support Interference and Flow Field Measurements*, AGARD CP-535, Oct. 1993, pp. 21.1–21.14 (Paper 21).

[23]Smith, J., "A Method for Determining 2D Wall Interference on an Aerofoil from Measured Pressure Distributions Near the Walls and on the Model," National Aerospace Lab., NLR TR-81016U., Amsterdam, The Netherlands, Jan. 1981, pp. 4–7.

[24]Kline, S. J., and McClintock, F. A., "Describing Uncertainties in Simple-Sample Experiments," *Mechanical Engineering*, Vol. 75, Jan. 1953, pp. 3–8.

[25]Rogers, S., "Numerical Solution of the Incompressible Navier–Stokes Equations," NASA TM-102199, Nov. 1990, pp. 1–35.

[26]Peyret, R., and Taylor, T. D., *Computational Methods for Fluid Flow*, Springer–Verlag, New York, 1983, pp. 144–171.

[27]Baldwin, B., and Barth, T., "A One-Equation Turbulence Transport Model for High Reynolds Number Wall-Bounded Flows," NASA TM-102847, Aug. 1990, pp. 1–19.

[28]Steinbrenner, J. P., Chawner, J. R., and Fouts, C. L., "The GRIDGEN 3D Multiple Block Grid Generation System, Vols. 1 and 2," U.S. Air Force Wright Research and Development Center, WRDC-TR-90-3022, Wright–Patterson AFB, OH, July 1990.

[29]Beutner, T., Celik, Z., and Roberts, L., "Determination of Solid/Porous Wall Boundary Conditions from Wind Tunnel Data for Computational Fluid Dynamics Codes," *Wall Interference, Support Interference and Flow Field Measurements*, AGARD CP-535, Oct. 1993, pp. 16.1–16.19 (Paper 16).

[30]Beutner, T., Celik, Z., and Roberts, L., "Modelling of Solid/Porous Wall Boundary Conditions for the Validation of Computational Fluid Dynamics Codes," AIAA Paper 92-0033, Jan. 1992.

[31]Beutner, T., Celik, Z., and Roberts, L., "Determination of Solid/Porous Wall Boundary Conditions from Wind Tunnel Data for Computational Fluid Dynamics Codes," AIAA Paper 93-0530, Jan. 1993.

J. Kallinderis
Associate Editor